

# THOM: Generating Physically Plausible Hand-Object Meshes From Text

Uyoung Jeong<sup>1</sup> Yihalem Yimolal Tiruneh<sup>1</sup>  
 Hyung Jin Chang<sup>2</sup> Seungryul Baek<sup>1</sup> Kwang In Kim<sup>3</sup>  
<sup>1</sup>UNIST <sup>2</sup>University of Birmingham <sup>3</sup>POSTECH

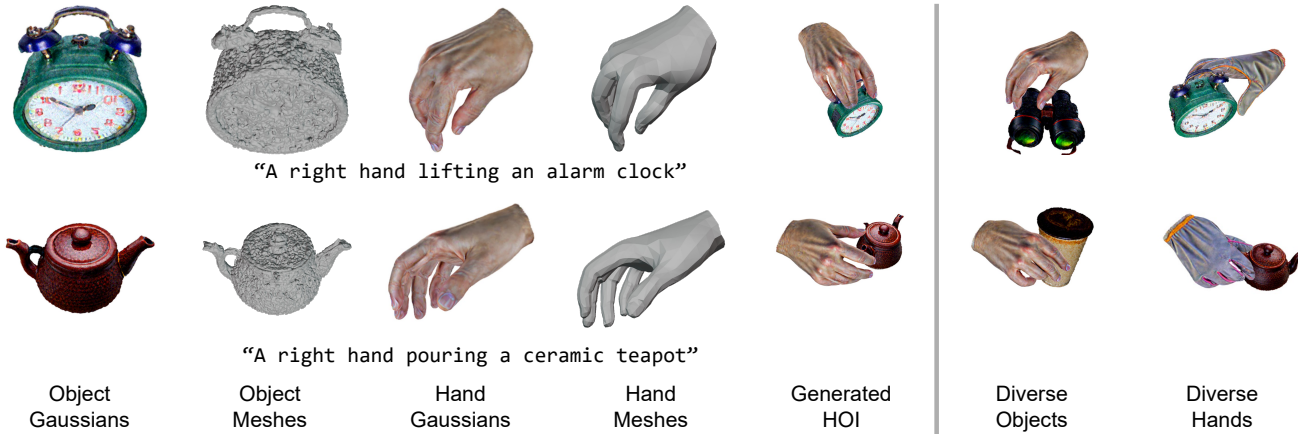


Figure 1. **THOM** is a novel photorealistic text-to-3D HOI generation pipeline that generalizes to diverse objects, hands and interactions.

## Abstract

The generation of 3D hand-object interactions (HOIs) from text is crucial for dexterous robotic grasping and VR/AR content generation, requiring both high visual fidelity and physical plausibility. Nevertheless, the ill-posed problem of mesh extraction from text-generated Gaussians, and physics-based optimization on the erroneous meshes pose challenges. To address these issues, we introduce **THOM**, a training-free framework that generates photorealistic, physically plausible 3D HOI meshes without the need for a template object mesh. **THOM** employs a two-stage pipeline, initially generating the hand and object Gaussians, followed by physics-based HOI optimization. Our new mesh extraction method and vertex-to-Gaussian mapping explicitly assign Gaussian elements to mesh vertices, allowing topology-aware regularization. Furthermore, we improve the physical plausibility of interactions by VLM-guided translation refinement and contact-aware optimization. Comprehensive experiments demonstrate that **THOM** consistently surpasses state-of-the-art methods in terms of text alignment, visual realism, and interaction plausibility.

## 1. Introduction

Generating photorealistic 3D hand-object interactions (HOIs) from text is a fundamental yet challenging task for dexterous robotic grasping [30, 35, 66, 83], collaborative robotics [42, 82], and AR/VR content creation [28, 84]. It generates diverse object shapes and their corresponding hand-object interactions directly from text, without requiring reference 3D object assets. This significantly lowers the barrier for non-expert users to generate diverse interactions simply from text prompts.

Despite its application value, there are three key technical challenges that are unique to this text-based photorealistic HOI generation task: (1) A lack of object and interaction diversity hinders the application of data-hungry learning-based approaches. While existing learning-based text-to-3D generation methods [61, 69, 71] are trained on the Objaverse dataset [11] containing  $\sim 818\text{K}$  objects with 21K classes, 3D HOI datasets consist of a few dozen object classes [14, 18, 58], which hinders training with large-scale generation models. (2) Existing optimization-based HOI generation methods [2, 10] use NeRF-based implicit volumes, lacking explicit mesh representations for physics-based HOI optimization. (3) Existing methods [4, 31] use physics-based HOI losses on watertight template ob-

ject meshes, and are therefore incapable of optimizing non-watertight object meshes generated from text.

To address the aforementioned challenges, we propose **THOM**, a training-free framework that generates diverse photorealistic HOI meshes from text with high physical plausibility (Fig. 1). First, to overcome the training data shortage issue, we take a per-sample optimization strategy, leveraging the generalization power of a text-to-image diffusion model and the representational efficiency of 3D Gaussians. Second, for robust physics-based HOI refinement coupled with volumetric rendering, THOM establishes explicit vertex-to-Gaussian mapping that facilitates physics-based HOI optimization. To address the limitations of previous mesh extraction methods that involve complex iterative refinement processes, we design a simplified object mesh extraction process. For robust HOI optimization, we further extract a lightweight and concise object mesh for efficient and accurate vertex normal estimation. Third, our robust physics-based HOI optimization process improves interaction plausibility on noisy text-generated object meshes. Our distance-adaptive masking strategy and reposition loss robustly align hand joints on the surfaces of diverse objects, thereby improving physical plausibility.

To further improve text-3D HOI alignment, we additionally refine hand translation using the high-level visual grounding capability of an existing vision-language model (VLM). Instead of resource-intensive fine-tuning [9, 32] or adding extra networks [22, 33], we utilize an existing open-source VLM without any training or modification. We prompt a VLM with rendered images of multiple candidates with different hand translations, and ask it to select the candidate with the best alignment.

Our contributions are summarized as follows:

- We generate photorealistic 3D HOI meshes with diverse shapes directly from text prompts.
- Our vertex-Gaussian mapping and simplified object mesh extraction enable accurate physics-based optimization.
- We achieve high physical plausibility via VLM-guided translation refinement and physics-based optimization with distance-adaptive masking and joint reposition loss.
- Comprehensive experiments demonstrate superior visual realism under diverse object and hand shapes, with improved physical plausibility compared to SOTA methods.

## 2. Related work

**Text-to-3D object generation.** Recent works on text-to-3D generation can be broadly categorized into three types: per-object optimization, multi-view 2D-to-3D lifting, and Large Reconstruction Model (LRM). DreamFusion [53] and subsequent works [5, 43, 45, 63] apply Score Distillation Sampling (SDS) to NeRF [46] renderings using a 2D image diffusion model as a prior. More recent methods [7, 34, 59, 75, 76] replace NeRF with Gaussian Splat-

ting [27] and further improve the optimization speed and memory usage. However, they struggle to accurately reconstruct human anatomy, particularly hands, and are not tailored for physically plausible hand-object interactions.

2D-to-3D lifting approaches divide the task into separate sub-tasks: 2D image generation and subsequent 3D lifting. Zero-1-to-3 [40], CAT3D [15] and related works [37, 38, 70] use multi-view images to obtain view-consistent 3D representations. SAM 3D [6] and Hunyuan3D 2.5 [29] further improve reconstruction fidelity with large-scale architectures and massive data. However, they fail to model articulated hands or produce physically plausible interactions.

LRM-based approaches [8, 39, 61, 69, 71] adopt learning-based methods to generate 3D objects. MeshFormer [39] employs 3D sparse convolutions and transformers to generate 3D representations. However, these methods often require extensive training costs on large-scale data. Similar to the lifting methods, these approaches also struggle to generate complex articulated content and lack explicit modeling of physical contact and penetration.

**Human/hand-object interaction generation.** Learning-based approaches [4, 12, 16, 74, 81] generate hand-object motions from the given object meshes. Although they offer a reasonable initialization prior, generalization to unseen object categories and shapes remains limited. In addition, they are unable to generate photorealistic scenes, and require template object meshes for HOI generation. On the other hand, our method generates photorealistic 3D Gaussians and their meshes from text without the need for the template object meshes and training data.

InterFusion [10] and DreamHOI [85] take a per-instance optimization approach, generating 3D human-object interactions by optimizing NeRF volumes. However, these methods suffer from low-resolution renderings due to the computational cost of NeRF volumetric grid representation. Moreover, these approaches lack contact-awareness, resulting in physically implausible interactions.

There are several 2D HOI image generation approaches. Affordance Diffusion [73] and DiffusionHOI [79] achieve this by training diffusion models on HOI datasets. While they are confined to generating 2D images and require computationally demanding training, our method generates photorealistic 3D HOIs without a learning-based approach.

**Mesh extraction from volumetric representations.** NeRF-based methods [36, 48, 60, 64] usually employ the iterative Marching Cubes algorithm to extract meshes, suffering from slow extraction speed and surface artifacts. Under Gaussian Splatting representation, SuGaR [17] performs Poisson reconstruction [26] by sampling point clouds from multi-view renderings, and binds Gaussians to triangles. Although faster than Marching Cubes, it requires heuristic

$y^{\text{hoi}}$  = "A right hand wearing a bracelet using pink headphones",  $y^{\text{obj}}$  = "Pink headphones",  $y^{\text{hand}}$  = "A right hand wearing a bracelet"

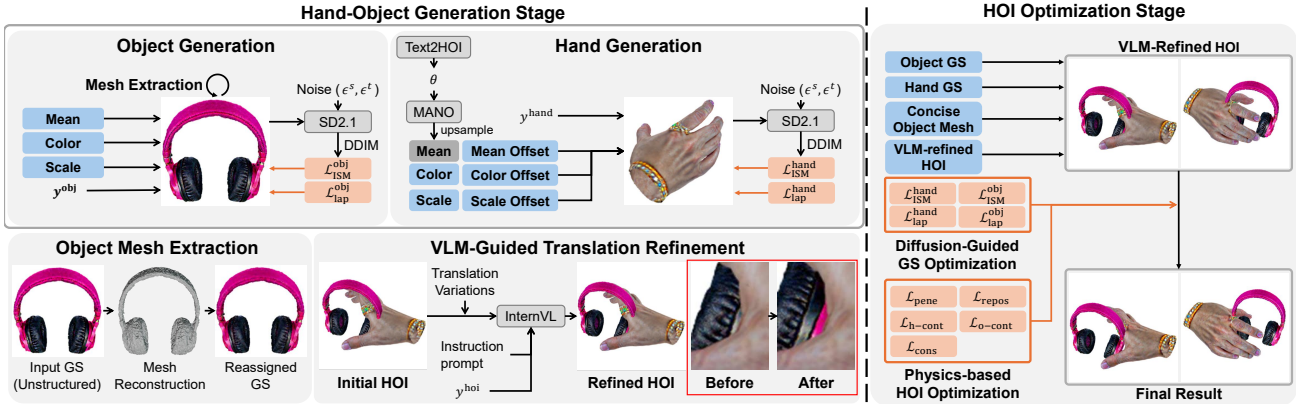


Figure 2. Overall pipeline of THOM. In the first stage, object and hand Gaussians are separately generated from the text prompts. During the second stage, we jointly refine the HOI Gaussians and HOI parameters. At HOI initialization, we refine the hand translation with VLM-guided refinement. During HOI parameters optimization, we introduce physics-based optimization via distance-adaptive contact losses and reposition loss. For both the first and the second stage, Laplacian regularization is applied for topological consistency.

tuning of the Gaussian counts, resulting in bumpy or incomplete surfaces and demanding extensive iterations. Our method, THOM, simplifies mesh extraction through direct Poisson reconstruction followed by vertex-based Gaussian upsampling, enabling explicit topological regularization on the Gaussians that preserves consistent 3D structure during optimization. For precise contact calculation, we additionally extract concise meshes from our reconstruction results.

**VLMs for 3D reasoning.** 3D reasoning or grounding using VLMs is an actively studied field. Existing methods either finetune VLMs on task-specific data [9, 32, 57, 68] or introduce additional modules to refine VLM outputs [1, 80], but both require annotated datasets and expensive training with limited generalizability. Recently, training-free methods have emerged [22, 33, 77] that directly utilize VLMs for 3D reasoning tasks. Motivated by these works, we propose a simple plug-and-play hand translation refinement strategy that requires no training or model modification.

### 3. Method

As illustrated in Fig. 2, our THOM framework adopts a two-stage pipeline for generating photorealistic 3D HOIs. Initially, object and hand meshes are independently generated with high visual realism. In the second stage, we jointly optimize their interaction parameters using physics-based losses for plausible contacts and minimal penetration.

#### 3.1. Diffusion guidance for 3D HOI generation

To generate 3D HOIs using a pretrained text-to-2D image diffusion model, we employ Interval Score Matching (ISM) loss, a variant of Score Distillation Sampling (SDS)

loss [34]. ISM loss provides more realistic and detailed results compared to SDS loss. Following GaussianDreamerPro [76], we calculate the ISM gradient using a DDIM scheduler. Using a diffusion model  $\phi$ , we compute the gradient for the Gaussian parameters  $\psi$  as:

$$\nabla_{\psi} \mathcal{L}_{\text{ISM}}(\phi, \mathcal{R}) \triangleq \mathbb{E}_{t, \epsilon} \left[ w(t) (\hat{\epsilon}_{\phi}(\mathcal{R}_t; x_t, t) - \hat{\epsilon}_{\phi}(\mathcal{R}_s; \emptyset, s)) \frac{\partial \mathcal{R}}{\partial \psi} \right], \quad (1)$$

where  $\mathcal{R}$  denotes the rendered Gaussian image,  $w(t)$  is a time scheduling weight, and  $t \in [2, 980]$  is a timestep.  $s (< t)$  is a timestep for inversion, and  $\emptyset$  is an empty text prompt.

#### 3.2. Vertex-Gaussian model

In hand-object generation, we adopt vertex-Gaussian mapping to maintain consistent topology that enables precise contact computation in the later HOI optimization stage.

**Object Gaussian model.** Given an object prompt  $y^o$ , the object Gaussians  $G^o$  are optimized using the guidance loss  $\mathcal{L}_{\text{guid}}$ . The Gaussians are parameterized by position  $\mu \in \mathbb{R}^{N \times 3}$ , scale  $s \in \mathbb{R}^{N \times 3}$ , color  $\mathbf{c} \in \mathbb{R}^{N \times 3}$ , opacity  $\alpha \in \mathbb{R}^{N \times 1}$ , and quaternion  $\mathbf{q} \in \mathbb{R}^{N \times 4}$ , where  $N$  is the number of Gaussians. We control the number of Gaussians to balance rendering fidelity and computational efficiency. Prior to mesh reconstruction, our object Gaussians have at most  $N = 800,000$  Gaussians. After reconstruction, the Gaussians are reinitialized with the mesh vertices, resulting in  $N' \approx 400,000$  elements.

**Hand Gaussian model.** Following the object Gaussian model, the hand Gaussian model  $G^h$  is optimized by  $\mathcal{L}_{\text{guid}}$

based on a hand text prompt  $y^h$ . Inspired by recent Gaussian avatar methods [20, 47, 52], we adopt the parametric MANO hand model [56] for Gaussian initialization. Specifically, the MANO mesh is upsampled fourfold to 196,993 vertices. The Gaussian positions are computed via pose-dependent transformations defined as below:

$$\mathbf{M}^h(\beta, \theta, \Delta\mu^h) = W(\mathbf{T}(\beta, \theta, \Delta\mu^h), \mathbf{J}(\beta), \theta, \mathcal{W}), \quad (2)$$

$$\mathbf{T}(\beta, \theta, \Delta\mu^h) = \bar{\mathbf{T}} + B_S(\beta) + B_P(\theta) + \Delta\mu^h, \quad (3)$$

where  $W$  is a linear blend skinning function,  $\mathbf{T}$  is a transformation of a template mesh  $\bar{\mathbf{T}}$  by a given hand pose  $\theta$  and hand shape  $\beta$  parameters.  $B_S$  and  $B_P$  are blend shape functions,  $\mathbf{J}$  is a set of hand joints, and  $\mathcal{W}$  is a blend weight matrix. We set  $\beta$  to 0 for simplicity. The position offset  $\Delta\mu^h$  enables per-vertex deformation of the Gaussian positions from the original MANO mesh.

In addition to position offsets, we optimize for Gaussian color and scale, denoted as  $\Delta\mathbf{c}$  and  $\Delta\mathbf{s}$ , respectively. The final color and scale of the Gaussians are computed by adding respective offsets:  $\mathbf{c}^h = \mathbf{c}^h + \Delta\mathbf{c}^h$ ,  $\mathbf{s}^h = \mathbf{s}^h + \Delta\mathbf{s}^h$ .

**Direct object mesh reconstruction.** Existing mesh extraction methods face challenges on text-generated object meshes, requiring an extensive refinement process [17, 48, 64]. We simplify the mesh extraction to Poisson reconstruction followed by vertex upsampling. Specifically, we upsample the object vertices to the target number  $N_{\text{obj}}^{\text{tgt}} = 400,000$ . Our simple yet effective method inherently ensures exact geometric alignment between mesh vertices and their corresponding Gaussian representations. To stop the noisy text-generated meshes from degrading vertex normal estimation, we further extract a concise mesh via farthest point sampling and alpha shape reconstruction [13], which is used for the contact and reposition losses in Sec. 3.3.

**One-to-one vertex-Gaussian mapping.** Our proposed mesh reconstruction preserves mesh topology, establishing a one-to-one vertex-Gaussian mapping by design. While previous NeRF-based [36, 67] or triangle-bind [17] approaches lack explicit geometric relationships between volumetric representations and the mesh, our method directly assigns each mesh vertex as a Gaussian. This structural correspondence bridges 3DGS with mesh-based physics optimization, allowing accurate penetration and contact computation without any auxiliary processing.

**Vertex-Gaussian topology regularization.** Due to the under-constrained nature of SDS-based optimization, generated Gaussians can exhibit floating artifacts and inconsistent appearance. Our vertex-Gaussian mapping naturally enables topological regularization, which is widely used in meshes [41, 47] but previously inapplicable to volumetric

3D generations. Specifically, we apply Laplacian regularization on Gaussian positions  $\mu$ , colors  $\mathbf{c}$ , and scales  $\mathbf{s}$ , enforcing local smoothness by leveraging the vertex topology:

$$\mathbf{L}(\mathbf{x}) = \mathbf{x} - \sum_{k=1}^K \mathbf{x}_{(\cdot, j_k)} \mathbf{W}_{(\cdot, k)}, \quad (4)$$

where  $\mathbf{W} \in \mathbb{R}^{N \times K}$  defines adjacency-weight matrix for top- $K$  nearest neighbors, and  $j_k$  denotes the vertex index.

For Gaussian color  $\mathbf{c}$  and scale  $\mathbf{s}$  parameters, we directly minimize their respective Laplacians to enforce local consistency. For Gaussian positions  $\mu$ , we match their Laplacian to that of the reference mesh vertices  $\mathbf{V}$ , preserving consistent topology. The comprehensive Laplacian regularization loss is defined as:

$$\mathcal{L}_{\text{lap}} = \lambda_{\text{lap}, \mu} (\mathbf{L}(\mu) - \mathbf{L}(\mathbf{V}))^2 + \lambda_{\text{lap}, \mathbf{c}} \mathbf{L}(\mathbf{c})^2 + \lambda_{\text{lap}, \mathbf{s}} \mathbf{L}(\mathbf{s})^2, \quad (5)$$

where  $\lambda_{\text{lap}, \mu}$ ,  $\lambda_{\text{lap}, \mathbf{c}}$ ,  $\lambda_{\text{lap}, \mathbf{s}}$  are the scalar weights. This topological regularization is consistently employed throughout the optimization pipeline, excluding only the initial phase of object Gaussian generation prior to mesh reconstruction.

To summarize, the optimization losses of the first stage for the object and the hand Gaussians are defined as follows:

$$\mathcal{L}_{\text{stage1}}^o = \mathcal{L}_{\text{ISM}}^o(\phi, \mathcal{R}^o) + \mathcal{L}_{\text{lap}}^o(\mu^o, \mathbf{V}^o, \mathbf{c}^o, \mathbf{s}^o), \quad (6)$$

$$\mathcal{L}_{\text{stage1}}^h = \mathcal{L}_{\text{ISM}}^h(\phi, \mathcal{R}^h) + \mathcal{L}_{\text{lap}}^h(\mu^h, \mathbf{V}^h, \mathbf{c}^h, \mathbf{s}^h), \quad (7)$$

where  $\mathcal{L}_{\text{lap}}^o$  is applied after the object mesh reconstruction.

### 3.3. Hand-object interaction optimization

**HOI Gaussians initialization.** Our final objective is to combine the generated hand and object Gaussians with plausible interaction. To construct a HOI Gaussian model  $G^{\text{hoi}}$ , we define HOI parameters  $\psi^{\text{hoi}}$  as below:

$$\psi^{\text{hoi}} = (\mathbf{r}^{\text{hoi}}, \mathbf{t}^{\text{hoi}}, \theta), \quad (8)$$

where  $\mathbf{r}^{\text{hoi}} \in \mathbb{R}^{1 \times 3}$  refers to the hand-relative object rotation in axis-angle format,  $\mathbf{t}^{\text{hoi}} \in \mathbb{R}^{1 \times 3}$  refers to the relative hand translation. Subsequently, we define the positions of the HOI Gaussians as follows:

$$\mu^{\text{hoi}} = (s\mu^h(\mathbf{R}^{\text{hoi}})^\top + \mathbf{t}^{\text{hoi}}, \mu^o), \quad (9)$$

where  $\mathbf{R}^{\text{hoi}}$  is a  $3 \times 3$  rotation matrix obtained from  $\mathbf{r}^{\text{hoi}}$ . We similarly apply transformation on the object Gaussian scalings and rotations using HOI parameters. HOI parameters and the interacting hand pose are initialized with Text2HOI [4]. To optimize the Gaussians, we separately

render the hand and object Gaussians without HOI parameters, and supervise with ISM loss. The total losses for HOI Gaussians optimization are defined as follows:

$$\mathcal{L}_{\text{hoi-GS}} = \mathcal{L}_{\text{ISM}}^{\text{h}} + \mathcal{L}_{\text{ISM}}^{\text{o}} + \mathcal{L}_{\text{lap}}^{\text{h}} + \mathcal{L}_{\text{lap}}^{\text{o}}, \quad (10)$$

where we omit the input arguments for simplicity. Note that we do not optimize ISM loss from the composited scene, since it leads to color mixing on the hand-object contact region, degrading fidelity.

**VLM-guided HOI refinement.** Although our physics-based HOI optimization in the later stage effectively improves physical plausibility, it does not ensure everything is in its right place, as it might produce misaligned hand positions by prioritizing penetration minimization without contextual understanding. To better align 3D and text with high-level HOI understanding, we utilize a vision-language model (VLM) for hand translation refinement before physics-based optimization.

Inspired by [22], we prompt an existing open-source VLM (InternVL3.5-14B [65]) to select the most plausible hand translation from the set of rendered images. Specifically, we generate 125(= 5 × 5 × 5) candidates by adding offsets in the range {−2, −1, 0, 1, 2}, each scaled by 1.0 × 10<sup>−2</sup>, to the initial 3D translation along the three Cartesian axes. We then instruct the VLM to select the most plausible sample by comparing multiple candidates based on the rendered images. For memory efficiency, we conduct the iterative selection process with a mini-batch of 3 images, repeating the process until only one candidate remains.

**Physics-based HOI optimization.** Thanks to our vertex-Gaussian representation and novel mesh extraction method, we can apply physics-based HOI optimization in our framework. To optimize the HOI parameters, we use several regularization losses as defined below:

$$\begin{aligned} \mathcal{L}_{\text{hoi-phys}} = & \lambda_{\text{pene}} \mathcal{L}_{\text{pene}} + \lambda_{\text{hc}} \mathcal{L}_{\text{hc}} \\ & + \lambda_{\text{oc}} \mathcal{L}_{\text{oc}} + \lambda_{\text{repos}} \mathcal{L}_{\text{repos}} + \lambda_{\text{cons}} \mathcal{L}_{\text{cons}}, \end{aligned} \quad (11)$$

where these losses do not require rendering, as they are directly calculated from the geometric properties of the vertex-Gaussians.  $\lambda$  represents the scalar weights for the respective losses. Extending from [25], we use penetration loss and mask-based contact losses as defined below:

$$\mathcal{L}_{\text{pene}}(\mathbf{n}^{\text{h}}, \mu^{\text{h}}, \mu^{\text{o}}) = \|\mu_{\text{pene}}^{\text{h}} - \mu_{\text{pene}}^{\text{o}}\|_F^2, \quad (12)$$

$$\mathcal{L}_{\text{oc}}(\mathbf{n}^{\text{h}}, \mu^{\text{h}}, \mu^{\text{o}}) = \|\mathbf{C}_{\text{o}} \odot (\mu_{\text{oc}}^{\text{o}} - \mu_{\text{oc}}^{\text{h}})\|_F^2, \quad (13)$$

$$\mathcal{L}_{\text{hc}}(\mathbf{n}_{\text{con}}^{\text{o}}, \mu_{\text{con}}^{\text{o}}, \mu^{\text{h}}) = \|\mathbf{C}_{\text{h}} \odot (\mu_{\text{hc}}^{\text{o}} - \mu_{\text{hc}}^{\text{h}})\|_F^2, \quad (14)$$

where  $\odot$  denotes the Hadamard product,  $\|\cdot\|_F$  is the Frobenius norm.  $\mu_{\text{pene}}^{\text{o}} \in \mathbb{R}^{N_{\text{pene}} \times 3}$  and  $\mu_{\text{pene}}^{\text{h}} \in \mathbb{R}^{N_{\text{pene}} \times 3}$  represent

the object and the nearest hand Gaussian positions in penetration, obtained by computing the dot product between the hand vertex normals ( $\mathbf{n}^{\text{h}}$ ) and  $\mathbf{v}^{\text{o} \rightarrow \text{h}} = \mu^{\text{h}} - \mu^{\text{o}}$ .  $\mu_{\text{oc}}^{\text{o}}$  and  $\mu_{\text{oc}}^{\text{h}}$  denote the object vertices and the nearest hand vertices.  $\mathbf{C}_{\text{o}}$  is a binary mask for the object vertices where the contacting vertex indices (across  $x, y, z$ -dimensions) are set to 1.  $\mu_{\text{hc}}^{\text{h}} \in \mathbb{R}^{21 \times 3}$  and  $\mu_{\text{hc}}^{\text{o}} \in \mathbb{R}^{21 \times 3}$  denote the hand joint positions and the nearest object vertices. Note that both  $\mathbf{C}_{\text{o}}$  and  $\mathbf{C}_{\text{h}}$  are initialized only once and do not change afterward.

Object vertex contact loss  $\mathcal{L}_{\text{oc}}$  minimizes the distance between the contacting object vertices and the nearest hand vertices. During initialization of  $\mathbf{C}_{\text{o}}$ , we set the penetrating object vertices as contact points. If there is no penetration, the closest top-5 object vertices are marked as contact points. Compared to previous work [24, 73], this loss effectively maps the contact affordance of the object without a time-consuming process.

Hand joint contact loss  $\mathcal{L}_{\text{hc}}$  penalizes distance between the contact hand joints and the nearest object vertices. During contact calculation, object vertex normals are required. Existing works [4, 25] assume watertight template meshes, thus failing on noisy text-generated meshes. Therefore, we revisit  $\mathcal{L}_{\text{hc}}$  in two aspects. First, we use the concise object mesh for precise and robust object vertex normal estimation. Second, we adapt the mask  $\mathbf{C}_{\text{h}}$  to mark the top-5 hand keypoints closest to the object vertices as contact joints, improving joint-level contact alignment on noisy object surfaces. These design choices effectively address the unique challenges of the text-to-HOI generation task.

**Reposition loss.** While the aforementioned losses improve overall physical plausibility, they do not explicitly relocate the penetrating hand joints to the object surface. They often bypass the optimization by simply pushing the hand apart from the object without modifying the hand poses. To address this issue, we explicitly guide the penetrating hand joints to be closer to the nearest object surfaces, when at least one of the following two criteria is satisfied: (1) A joint is inside the concise object mesh. (2) A joint is marked as a contact joint. For these joints, we compute L2 loss between the current MANO joint and the nearest concise object vertex positions, defined as follows:

$$\mathcal{L}_{\text{repos}}(\mathbf{n}_{\text{con}}^{\text{o}}, \mu_{\text{con}}^{\text{o}}, \mathbf{J}) = \|\mathbf{J}_{\text{repos}} - \mu_{\text{repos}}^{\text{o}}\|_F^2, \quad (15)$$

where  $(\mathbf{J}_{\text{repos}}, \mu_{\text{repos}}^{\text{o}}) \in \mathbb{R}^{\#\text{repos} \times 3}$ . Similar to Eq. (14), we use vertex normals of the concise object for robust hand joint penetration estimation.

**Consistency loss.**  $\mathcal{L}_{\text{cons}}$  regularizes the HOI parameters to prevent collapse:

$$\begin{aligned} \mathcal{L}_{\text{cons}}(\mathbf{t}, \mathbf{r}, \theta) = & \|\mathbf{t}^{\text{hoi}} - \mathbf{t}_{\text{init}}^{\text{hoi}}\|^2 + \|\mathbf{r}^{\text{hoi}} - \mathbf{r}_{\text{init}}^{\text{hoi}}\|^2 \\ & + \|\mathbf{W}_{xy} \odot (\theta - \theta_{\text{init}})\|_F^2, \end{aligned} \quad (16)$$

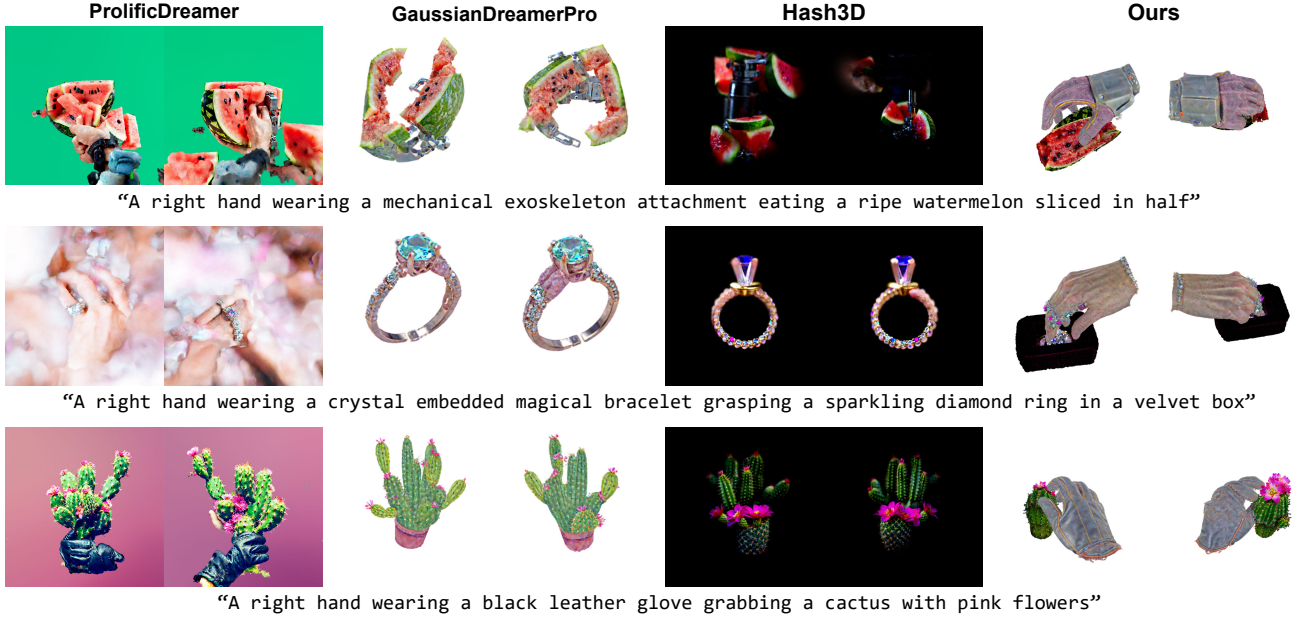


Figure 3. Qualitative comparisons of ProlificDreamer [67], GaussianDreamerPro [76], Hash3D [72] and ours.

Table 1. Comparison with state-of-the-art text-to-3D methods and text-to-3D human-object interaction generation methods. \*: Adapted to generate hand-object interactions.

Method	Time	CLIP	T <sup>3</sup> -Align
DreamFusion [53]	35 min.	27.1	1.3
ProlificDreamer [67]	3 hours	29.1	1.2
GaussianDreamerPro [76]	1 hour 30 min.	28.5	1.4
Hash3D [72]	25 min.	27.6	1.9
InterFusion* [10]	2 hour	22.5	1.5
DreamHOI* [85]	3 hour 20 min.	27.8	1.6
Ours	2 hour 30 min.	<b>31.4</b>	<b>2.6</b>

where  $\mathbf{t}_{\text{init}}^{\text{hoi}}$ ,  $\mathbf{r}_{\text{init}}^{\text{hoi}}$ ,  $\theta_{\text{init}}$  are the initial parameter values.  $\mathbf{W}_{xy}$  applies  $10\times$  stronger penalization on the x- and y-axes, which govern left/right and horizontal joint rotations that are anatomically constrained, whereas the z-axis controls finger flexion and is less restricted.

## 4. Experiments

### 4.1. Implementation details

We generate 3D HOIs from input text prompts through two stages. **Stage 1:** Object and hand Gaussians are independently generated for 7,000 iterations. For the object Gaussians, mesh extraction is performed at the 5,000th iteration, followed by subsequent optimization with Laplacian regularization. To guarantee visibility, we enforce a minimum opacity of 0.5 for object Gaussians and 1.0 for hand

Table 2. Physics and simulation evaluation results with learning-based HOI generation methods.

Method	Max. pene.↓	Mean. pene.↓	Contact ratio↑	Disp.↓
G-HOP	$1.30\times 10^{-2}$	$9.52\times 10^{-3}$	0.15	1.00
Text2HOI	$5.16\times 10^{-4}$	$2.28\times 10^{-4}$	<b>0.98</b>	0.25
Ours	<b><math>2.20\times 10^{-5}</math></b>	<b><math>1.24\times 10^{-5}</math></b>	0.95	<b>0.20</b>

Gaussians. **Stage 2:** HOI parameters are initialized using Text2HOI [4] and the translation parameter is refined with VLM. Then, the hand-object Gaussians and their HOI parameters are optimized for 1,000 iterations. The object Gaussian position parameters are frozen for stable contact refinement. The Gaussians and HOI parameters are separately optimized by different optimizers to avoid suboptimal visual quality due to physics-based objectives. Experiments are conducted on a single NVIDIA RTX 3090 GPU. The first stage takes approximately two hours, and the second stage takes around 30 minutes.

### 4.2. Evaluation criteria

To assess the generalization capability of our framework, we evaluate it on 100 different text prompts with 24 diverse action types. We use the object prompts from T<sup>3</sup>Bench [19] for object generation, and we generate 100 hand prompts with diverse appearances using GPT-4o [23]. Hand and object prompts are manually paired to ensure plausible interactions. Our evaluation set significantly exceeds previ-

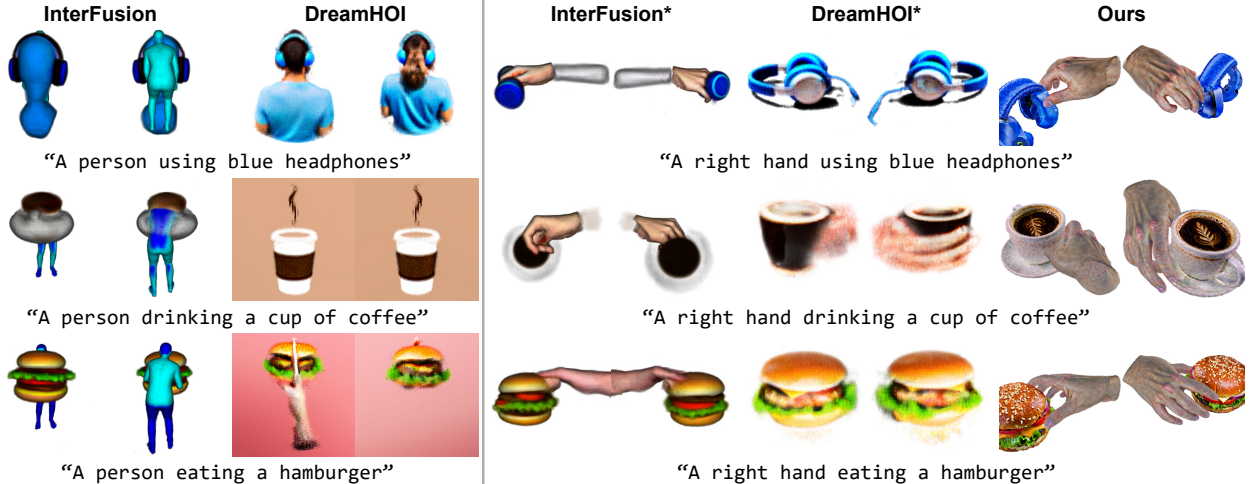


Figure 4. Qualitative comparison with human-object interaction methods. \*: Adapted to generate hand-object interactions.

Table 3. Ablation results with CLIP score. Higher scores indicate better performance. Our complete method shows the best score.

w/o $\mathcal{L}_{lap}$	w/o $\mathcal{L}_{hoi-phys}$	w/o $\mathcal{L}_{repos}$	w/o VLM	all
30.4	30.3	31.0	31.3	<b>31.4</b>

ous benchmarks, such as InterFusion with 61 prompts and DreamHOI with 12 prompts.

We use CLIP score [54] to evaluate the alignment between the input HOI text prompt and the rendered images, similar to the related works [10, 21]. We further evaluate image-text alignment using T<sup>3</sup>Bench Alignment metric [19]. While GPT-4V select metric used in InterFusion and DreamHOI is a relative evaluation protocol, T<sup>3</sup>-Alignment metric is an absolute evaluation protocol and therefore independent of the comparative baselines.

### 4.3. Comparative results

#### 4.3.1. Quantitative results

To the best of our knowledge, there is no directly comparable method, as THOM is the first method to generate *photorealistic* 3D hand-object interactions directly from text prompts in zero-shot. Therefore, we compare our method with SOTA text-to-3D and text-to-human-object interaction generation methods. Table 1 presents a comparative evaluation against SOTAs. Our method outperforms others by a significant margin, indicating stronger alignment with interaction prompts. Additionally, THOM significantly reduces generation time. While GaussianDreamerPro requires approximately three hours to generate two compositions, our method achieves the same in 30 minutes less and yields a 2.9-point higher CLIP score. Our method also outperforms

ProlificDreamer by a large margin, both in terms of CLIP score (2.3 $\uparrow$ ) and T<sup>3</sup>-Alignment (1.4 $\uparrow$ ). THOM also outperforms all SOTAs in T<sup>3</sup>-Alignment score by at least 0.7 points. Overall, the results suggest that our proposed framework is useful for generating high-fidelity HOIs.

We compare our method with SOTA zero-shot human-object interaction generation methods. Since they are not directly applicable to hands, we adapt their implementations to generate hand-object interactions. Modification details are provided in the supplementary material. In Tab. 1, we report quantitative comparison against InterFusion and DreamHOI. InterFusion and DreamHOI fail to generate high-fidelity and physically plausible results, as their implicit representations hinder accurate physics optimization. Our method significantly outperforms on both CLIP score and T<sup>3</sup>-Alignment score, indicating that our method excels at generating 3D HOIs.

To validate physical plausibility of our generation results, we compare with learning-based HOI mesh generation methods in Tab. 2. G-HOP and Text2HOI are trained from template object meshes and generate non-photorealistic HOIs, showing suboptimal performance on unseen text-generated object meshes. THOM significantly improves penetration by orders of magnitude, achieving the smallest penetration depths while maintaining a high contact ratio. Our method also effectively improves the displacement measured by PyBullet physics simulation.

#### 4.3.2. Qualitative results

Our method produces superior qualitative results. In Fig. 3, all state-of-the-art text-to-3D methods fail to generate hands with correct geometry. Specifically, ProlificDreamer suffers from background clutter and a severe multi-face problem. GaussianDreamerPro and Hash3D often fail to generate ob-

Table 4. Ablation of object mesh reconstruction methods.

Method	CLIP $\uparrow$	Pene. $\downarrow$
Downsample	30.9	$7.3 \times 10^{-5}$
Marching Cubes	26.8	$2.3 \times 10^{-5}$
SuGaR	30.4	$3.8 \times 10^{-5}$
Ours	<b>31.4</b>	<b><math>2.2 \times 10^{-5}</math></b>

Table 5. Ablation of physics optimization and VLM refinement using GPT-4o select metric. Values indicate the preference frequency (one sample excluded due to GPT-4o non-response).

w/o phys. opt	w/o VLM	Ours (all)
13	25	<b>61</b>

jects and hands separately, producing implausible results. In contrast, our method consistently generates high-fidelity 3D HOIs, with plausible interactions, showing a strong generalization capability.

In Fig. 4, we qualitatively compare with InterFusion and DreamHOI. Both InterFusion and DreamHOI fail to generate physically plausible interactions, due to the lack of explicit mesh representation and contact-awareness. InterFusion suffers from low-fidelity and cluttering artifacts. DreamHOI often fails to correctly generate hands, due to clutter in implicit NeRF volumes. On the other hand, our method consistently provides high-fidelity visual results along with plausible interactions.

#### 4.4. Ablation study

In Tab. 3, we demonstrate the effectiveness of our proposed methods. Removing the Laplacian loss (w/o  $\mathcal{L}_{lap}$ ) significantly drops the CLIP score by 1.0. It degrades the topological consistency of object and hand meshes, resulting in degraded colors and jittery surfaces. Omitting all physics-based losses (w/o  $\mathcal{L}_{hoi-phys}$ ) corresponds to using Text2HOI output without modification, resulting in a 1.1 point drop. The initial Text2HOI results suffer from significant interpenetration, undermining interaction plausibility. Removing only the reposition loss (w/o  $\mathcal{L}_{repos}$ ) also leads to a sub-optimal result, implying that reposition loss helps supervise the penetrating hand joints explicitly. We observe that the removal of VLM-guided refinement (w/o VLM) also drops the CLIP score by 0.1. VLM refinement largely improves T<sup>3</sup>-Align by 0.6 points compared to the non-VLM baseline (details are provided in the supplementary material).

We also provide ablation results on our mesh extraction method in Tab. 4. We replace our mesh extraction method with other methods and then apply HOI optimization. For Marching Cubes, we use point-E [50]. Our proposed mesh extraction method surpasses other baselines



Figure 5. VLM refinement results. Left: "A right hand calling a smartphone". Middle: "A right hand using a hammer". Right: "A right hand inspecting Paddington Bear".

in CLIP score and maximum penetration. Downsampling, which downsamples from the baseline SuGaR, shows the worst penetration, as it exhibits severe non-watertight topology. While artifacts in Marching Cubes and jittery triangle-bound SuGaR hinder accurate penetration and contact estimation, our method empowers robust HOI optimization.

In Tab. 5, we isolate the effects of physics optimization and VLM refinement. From 100 generation results, we ask GPT-4o to select the preferred generation result among 3 candidates. Directly using the Text2HOI results (w/o phys. opt) was the least preferred. Incorporating both the physics optimization and VLM refinement is the most preferred method, validating the effectiveness of our framework.

Fig. 5 shows qualitative results of VLM-guided refinement. The refinement moves the hand toward plausible contact (left), improves grasp alignment on the handle (middle), and reduces thumb-object interpenetration (right), demonstrating consistent improvements in interaction plausibility across diverse objects.

## 5. Conclusion

We present a novel text-to-3D HOI generation pipeline with high visual fidelity and physical plausibility. Our novel mesh extraction and vertex-Gaussian mapping enable us to exploit mesh topology for efficient optimization and high visual fidelity. Combined with VLM-guided translation refinement and physics-based losses (distance-adaptive contact losses and reposition loss), our method facilitates robust interaction refinement for diverse objects and hand shapes.

**Limitation.** While THOM achieves superior quality and fast generation compared to previous per-sample optimization approaches, its generation time is still longer than the learning-based methods. Future work could employ time-efficient diffusion models such as DeepCache [44].

**Acknowledgments.** This work was supported by the Institute of Information & Communications Technology Plan-

ning & Evaluation (IITP) grants (No. RS-2020-II201336, Artificial Intelligence Graduate School Program (UNIST); No. RS-2019-II191906, Artificial Intelligence Graduate School Program (POSTECH); No. RS-2022-II220290, Visual Intelligence for Space-Time Understanding and Generation), the National Research Foundation of Korea (NRF) grant (No. RS-2024-00337559), and the InnoCORE program (26-InnoCORE-01) of the Ministry of Science and ICT (MSIT), all funded by the Korea government (MSIT).

## References

- [1] Zhaochong An, Guolei Sun, Yun Liu, Runjia Li, Junlin Han, Ender Konukoglu, and Serge Belongie. Generalized few-shot 3d point cloud segmentation with vision-language model. In *CVPR*, pages 16997–17007, 2025. 3
- [2] Yukang Cao, Liang Pan, Kai Han, Kwan-Yee K. Wong, and Ziwei Liu. AvatarGO: Zero-shot 4d human-object interaction generation and animation. *arXiv preprint arXiv:2410.07164*, 2024. 1
- [3] Zhe Cao, Tomas Simon, Shih-En Wei, and Yaser Sheikh. Realtime multi-person 2d pose estimation using part affinity fields. In *CVPR*, 2017. 4
- [4] Junuk Cha, Jihyeon Kim, Jae Shin Yoon, and Seungryul Baek. Text2HOI: Text-guided 3d motion generation for hand-object interaction. In *CVPR*, pages 1577–1585, 2024. 1, 2, 4, 5, 6
- [5] Rui Chen, Yongwei Chen, Ningxin Jiao, and Kui Jia. Fantasia3d: Disentangling geometry and appearance for high-quality text-to-3d content creation. In *ICCV*, pages 22246–22256, 2023. 2
- [6] Xingyu Chen, Fu-Jen Chu, Pierre Gleize, Kevin J Liang, Alexander Sax, Hao Tang, Weiyao Wang, Michelle Guo, Thibaut Hardin, Xiang Li, et al. Sam 3d: 3dfy anything in images. *arXiv preprint arXiv:2511.16624*, 2025. 2
- [7] Zilong Chen, Feng Wang, Yikai Wang, and Huaping Liu. Text-to-3d using gaussian splatting. In *CVPR*, pages 21401–21412, 2024. 2
- [8] Zhaoxi Chen, Jiayang Tang, Yuhao Dong, Ziang Cao, Fangzhou Hong, Yushi Lan, Tengfei Wang, Haozhe Xie, Tong Wu, Shunsuke Saito, Liang Pan, Dahua Lin, and Ziwei Liu. 3DTopia-XL: High-quality 3d pbr asset generation via primitive diffusion. In *CVPR*, 2025. 2
- [9] An-Chieh Cheng, Hongxu Yin, Yang Fu, Qiushan Guo, Ruihan Yang, Jan Kautz, Xiaolong Wang, and Sifei Liu. Spatial-rgpt: Grounded spatial reasoning in vision-language models. *NeurIPS*, 37:135062–135093, 2024. 2, 3
- [10] Sisi Dai, Wenhao Li, Haowen Sun, Haibin Huang, Chongyang Ma, Hui Huang, Kai Xu, and Ruizhen Hu. InterFusion: Text-driven generation of 3d human-object interaction. In *ECCV*, 2024. 1, 2, 6, 7
- [11] Matt Deitke, Dustin Schwenk, Jordi Salvador, Luca Weihs, Oscar Michel, Eli VanderBilt, Ludwig Schmidt, Kiana Ehsani, Aniruddha Kembhavi, and Ali Farhadi. Objaverse: A universe of annotated 3d objects. In *CVPR*, pages 13142–13153, 2023. 1
- [12] Christian Diller and Angela Dai. Cg-hoi: Contact-guided 3d human-object interaction generation. In *CVPR*, pages 19888–19901, 2024. 2
- [13] Herbert Edelsbrunner, David Kirkpatrick, and Raimund Seidel. On the shape of a set of points in the plane. *IEEE Transactions on information theory*, 29(4):551–559, 2003. 4
- [14] Zicong Fan, Omid Taheri, Dimitrios Tzionas, Muhammed Kocabas, Manuel Kaufmann, Michael J Black, and Otmar Hilliges. ARCTIC: A dataset for dexterous bimanual hand-object manipulation. In *CVPR*, pages 12943–12954, 2023. 1, 5
- [15] Ruiqi Gao\*, Aleksander Holynski\*, Philipp Henzler, Arthur Brussee, Ricardo Martin-Brualla, Pratul P. Srinivasan, Jonathan T. Barron, and Ben Poole\*. CAT3D: Create anything in 3d with multi-view diffusion models. *NeurIPS*, 2024. 2
- [16] Anindita Ghosh, Rishabh Dabral, Vladislav Golyanik, Christian Theobalt, and Philipp Slusallek. IMoS: Intent-driven full-body motion synthesis for human-object interactions. In *Computer Graphics Forum*, pages 1–12. Wiley Online Library, 2023. 2
- [17] Antoine Guédon and Vincent Lepetit. Sugar: Surface-aligned gaussian splatting for efficient 3d mesh reconstruction and high-quality mesh rendering. In *CVPR*, pages 5354–5363, 2024. 2, 4
- [18] Shreyas Hampali, Mahdi Rad, Markus Oberweger, and Vincent Lepetit. Honnotate: A method for 3d annotation of hand and object poses. In *CVPR*, pages 3196–3206, 2020. 1
- [19] Yuze He, Yushi Bai, Matthieu Lin, Wang Zhao, Yubin Hu, Jenny Sheng, Ran Yi, Juanzi Li, and Yong-Jin Liu. T<sup>3</sup>Bench: Benchmarking current progress in text-to-3d generation, 2023. 6, 7, 5
- [20] Hezhen Hu, Zhiwen Fan, Tianhao Wu, Yihan Xi, Seoyoung Lee, Georgios Pavlakos, and Zhangyang Wang. Expressive gaussian human avatars from monocular rgb video. In *NeurIPS*, 2024. 4
- [21] Hanzhe Hu, Tianwei Yin, Fujun Luan, Yiwei Hu, Hao Tan, Zexiang Xu, Sai Bi, Shubham Tulsiani, and Kai Zhang. Turbo3D: Ultra-fast text-to-3d generation. *arXiv preprint arXiv:2412.04470*, 2024. 7
- [22] Ian Huang, Yanan Bao, Karen Truong, Howard Zhou, Cordelia Schmid, Leonidas Guibas, and Alireza Fathi. Fire-place: Geometric refinements of llm common sense reasoning for 3d object placement. In *CVPR*, pages 13466–13476, 2025. 2, 3, 5, 4
- [23] Aaron Hurst, Adam Lerer, Adam P Goucher, Adam Perelman, Aditya Ramesh, Aidan Clark, AJ Ostrow, Akila Welihinda, Alan Hayes, Alec Radford, et al. Gpt-4o system card. *arXiv preprint arXiv:2410.21276*, 2024. 6
- [24] Juntao Jian, Xiuping Liu, Manyi Li, Ruizhen Hu, and Jian Liu. Affordpose: A large-scale dataset of hand-object interactions with affordance-driven hand pose. In *ICCV*, pages 14713–14724, 2023. 5
- [25] Hanwen Jiang, Shaowei Liu, Jiashun Wang, and Xiaolong Wang. Hand-object contact consistency reasoning for human grasps generation. In *ICCV*, pages 11107–11116, 2021. 5

- [26] Michael Kazhdan, Matthew Bolitho, and Hugues Hoppe. Poisson surface reconstruction. In *Proceedings of the fourth Eurographics symposium on Geometry processing*, 2006. 2
- [27] Bernhard Kerbl, Georgios Kopanas, Thomas Leimkühler, and George Drettakis. 3d gaussian splatting for real-time radiance field rendering. *ACM Trans. Graph.*, 42(4):139–1, 2023. 2
- [28] ByungMin Kim, DongHeun Han, and HyeongYeop Kang. Shaping the future of vr hand interactions: Lessons learned from modern methods. In *2025 IEEE Conference Virtual Reality and 3D User Interfaces (VR)*, pages 165–174. IEEE, 2025. 1
- [29] Zeqiang Lai, Yunfei Zhao, Haolin Liu, Zibo Zhao, Qingxiang Lin, Huiwen Shi, Xianghui Yang, Mingxin Yang, Shuhui Yang, Yifei Feng, et al. Hunyuan3d 2.5: Towards high-fidelity 3d assets generation with ultimate details. *arXiv preprint arXiv:2506.16504*, 2025. 2
- [30] Kailin Li, Puhao Li, Tengyu Liu, Yuyang Li, and Siyuan Huang. Maniptrans: Efficient dexterous bimanual manipulation transfer via residual learning. In *CVPR*, pages 6991–7003, 2025. 1
- [31] Muchen Li, Sammy Christen, Chengde Wan, Yujun Cai, Renjie Liao, Leonid Sigal, and Shugao Ma. LatentHOI: On the generalizable hand object motion generation with latent hand diffusion. In *CVPR*, pages 17416–17425, 2025. 1
- [32] Peiyan Li, Yixiang Chen, Hongtao Wu, Xiao Ma, Xiangnan Wu, Yan Huang, Liang Wang, Tao Kong, and Tieniu Tan. BridgeVLA: Input-output alignment for efficient 3d manipulation learning with vision-language models. *arXiv preprint arXiv:2506.07961*, 2025. 2, 3
- [33] Rong Li, Shijie Li, Lingdong Kong, Xulei Yang, and Junwei Liang. Seeground: See and ground for zero-shot open-vocabulary 3d visual grounding. In *CVPR*, pages 3707–3717, 2025. 2, 3
- [34] Yixun Liang, Xin Yang, Jiantao Lin, Haodong Li, Xiaogang Xu, and Yingcong Chen. Luciddreamer: Towards high-fidelity text-to-3d generation via interval score matching. In *CVPR*, pages 6517–6526, 2024. 2, 3
- [35] Zhixuan Liang, Yao Mu, Yixiao Wang, Tianxing Chen, Wenqi Shao, Wei Zhan, Masayoshi Tomizuka, Ping Luo, and Mingyu Ding. Dexhanddiff: Interaction-aware diffusion planning for adaptive dexterous manipulation. In *CVPR*, pages 1745–1755, 2025. 1
- [36] Chen-Hsuan Lin, Jun Gao, Luming Tang, Towaki Takikawa, Xiaohui Zeng, Xun Huang, Karsten Kreis, Sanja Fidler, Ming-Yu Liu, and Tsung-Yi Lin. Magic3d: High-resolution text-to-3d content creation. In *CVPR*, pages 300–309, 2023. 2, 4
- [37] Minghua Liu, Chao Xu, Haian Jin, Linghao Chen, Mukund Varma T, Zexiang Xu, and Hao Su. One-2-3-45: Any single image to 3d mesh in 45 seconds without per-shape optimization. *NeurIPS*, 36:22226–22246, 2023. 2
- [38] Minghua Liu, Ruoxi Shi, Linghao Chen, Zhuoyang Zhang, Chao Xu, Xinyue Wei, Hansheng Chen, Chong Zeng, Jiayuan Gu, and Hao Su. One-2-3-45++: Fast single image to 3d objects with consistent multi-view generation and 3d diffusion. In *CVPR*, pages 10072–10083, 2024. 2
- [39] Minghua Liu, Chong Zeng, Xinyue Wei, Ruoxi Shi, Linghao Chen, Chao Xu, Mengqi Zhang, Zhaoning Wang, Xiaoshuai Zhang, Isabella Liu, Hongzhi Wu, and Hao Su. MeshFormer: High-quality mesh generation with 3d-guided reconstruction model. *NeurIPS*, 37:59314–59341, 2024. 2
- [40] Ruoshi Liu, Rundi Wu, Basile Van Hoorick, Pavel Tokmakov, Sergey Zakharov, and Carl Vondrick. Zero-1-to-3: Zero-shot one image to 3d object. In *ICCV*, pages 9298–9309, 2023. 2
- [41] Shichen Liu, Tianye Li, Weikai Chen, and Hao Li. Soft rasterizer: A differentiable renderer for image-based 3d reasoning. In *ICCV*, pages 7708–7717, 2019. 4
- [42] Yun Liu, Chengwen Zhang, Ruofan Xing, Bingda Tang, Bowen Yang, and Li Yi. Core4d: A 4d human-object-human interaction dataset for collaborative object rearrangement. In *CVPR*, pages 1769–1782, 2025. 1
- [43] Artem Lukoianov, Haitz Sáez de Ocáriz Borde, Kristjan Greenewald, Vitor Guizilini, Timur Bagautdinov, Vincent Sitzmann, and Justin M Solomon. Score distillation via reparametrized ddim. *NeurIPS*, 37:26011–26044, 2024. 2
- [44] Xinyin Ma, Gongfan Fang, and Xinchao Wang. Deepcache: Accelerating diffusion models for free. In *CVPR*, pages 15762–15772, 2024. 8
- [45] Gal Metzer, Elad Richardson, Or Patashnik, Raja Giryes, and Daniel Cohen-Or. Latent-nerf for shape-guided generation of 3d shapes and textures. In *CVPR*, pages 12663–12673, 2023. 2
- [46] Ben Mildenhall, Pratul P Srinivasan, Matthew Tancik, Jonathan T Barron, Ravi Ramamoorthi, and Ren Ng. Nerf: Representing scenes as neural radiance fields for view synthesis. *Communications of the ACM*, 65(1):99–106, 2021. 2
- [47] Gyeongsik Moon, Takaaki Shiratori, and Shunsuke Saito. Expressive whole-body 3d gaussian avatar. In *ECCV*, 2024. 4
- [48] Jacob Munkberg, Jon Hasselgren, Tianchang Shen, Jun Gao, Wenzheng Chen, Alex Evans, Thomas Müller, and Sanja Fidler. Extracting triangular 3d models, materials, and lighting from images. In *CVPR*, pages 8280–8290, 2022. 2, 4
- [49] Supreeth Narasimhaswamy, Uttaran Bhattacharya, Xiang Chen, Ishita Dasgupta, Saayan Mitra, and Minh Hoai. Handiffuser: Text-to-image generation with realistic hand appearances. In *CVPR*, pages 2468–2479, 2024. 3
- [50] Alex Nichol, Heewoo Jun, Prafulla Dhariwal, Pamela Mishkin, and Mark Chen. Point-e: A system for generating 3d point clouds from complex prompts. *arXiv preprint arXiv:2212.08751*, 2022. 8
- [51] Georgios Pavlakos, Dandan Shan, Ilija Radosavovic, Angjoo Kanazawa, David Fouhey, and Jitendra Malik. Reconstructing hands in 3D with transformers. In *CVPR*, 2024. 4
- [52] Chandradeep Pokhariya, Ishaan Nikhil Shah, Angela Xing, Zekun Li, Kefan Chen, Avinash Sharma, and Srinath Sridhar. Manus: Markerless grasp capture using articulated 3d gaussians. In *CVPR*, pages 2197–2208, 2024. 4
- [53] Ben Poole, Ajay Jain, Jonathan T Barron, and Ben Mildenhall. Dreamfusion: Text-to-3d using 2d diffusion. *arXiv preprint arXiv:2209.14988*, 2022. 2, 6

- [54] Alec Radford, Jong Wook Kim, Chris Hallacy, Aditya Ramesh, Gabriel Goh, Sandhini Agarwal, Girish Sastry, Amanda Askell, Pamela Mishkin, Jack Clark, et al. Learning transferable visual models from natural language supervision. In *ICML*, pages 8748–8763. PmLR, 2021. 7
- [55] Robin Rombach, Andreas Blattmann, Dominik Lorenz, Patrick Esser, and Björn Ommer. High-resolution image synthesis with latent diffusion models. In *CVPR*, pages 10684–10695, 2022. 4
- [56] Javier Romero, Dimitrios Tzionas, and Michael J. Black. Embodied Hands: Modeling and capturing hands and bodies together. *ACM Transactions on Graphics, (Proc. SIGGRAPH Asia)*, 36(6), 2017. 4
- [57] Fan-Yun Sun, Weiyu Liu, Siyi Gu, Dylan Lim, Goutam Bhat, Federico Tombari, Manling Li, Nick Haber, and Jiajun Wu. Layoutvlm: Differentiable optimization of 3d layout via vision-language models. In *CVPR*, pages 29469–29478, 2025. 3
- [58] Omid Taheri, Nima Ghorbani, Michael J Black, and Dimitrios Tzionas. GRAB: A dataset of whole-body human grasping of objects. In *ECCV*, pages 581–600. Springer, 2020. 1, 5
- [59] Jiaxiang Tang, Jiawei Ren, Hang Zhou, Ziwei Liu, and Gang Zeng. Dreamgaussian: Generative gaussian splatting for efficient 3d content creation. *arXiv preprint arXiv:2309.16653*, 2023. 2
- [60] Jiaxiang Tang, Hang Zhou, Xiaokang Chen, Tianshu Hu, Er-rui Ding, Jingdong Wang, and Gang Zeng. Delicate textured mesh recovery from nerf via adaptive surface refinement. In *ICCV*, pages 17739–17749, 2023. 2
- [61] Jiaxiang Tang, Zhaoxi Chen, Xiaokang Chen, Tengfei Wang, Gang Zeng, and Ziwei Liu. Lgm: Large multi-view gaussian model for high-resolution 3d content creation. In *ECCV*, pages 1–18. Springer, 2024. 1, 2
- [62] Masatoshi Tateno, Gido Kato, Hirokatsu Kataoka, Yoichi Sato, and Takuma Yagi. Handyvqa: A video qa benchmark for fine-grained hand-object interaction dynamics. *arXiv preprint arXiv:2512.00885*, 2025. 3
- [63] Haochen Wang, Xiaodan Du, Jiahao Li, Raymond A Yeh, and Greg Shakhnarovich. Score jacobian chaining: Lifting pretrained 2d diffusion models for 3d generation. In *CVPR*, pages 12619–12629, 2023. 2
- [64] Peng Wang, Lingjie Liu, Yuan Liu, Christian Theobalt, Taku Komura, and Wenping Wang. Neus: Learning neural implicit surfaces by volume rendering for multi-view reconstruction. *arXiv preprint arXiv:2106.10689*, 2021. 2, 4
- [65] Weiyun Wang, Zhangwei Gao, Lixin Gu, Hengjun Pu, Long Cui, Xingguang Wei, Zhaoyang Liu, Linglin Jing, Shenglong Ye, Jie Shao, et al. Internv13. 5: Advancing open-source multimodal models in versatility, reasoning, and efficiency. *arXiv preprint arXiv:2508.18265*, 2025. 5
- [66] Wenbo Wang, Fangyun Wei, Lei Zhou, Xi Chen, Lin Luo, Xiaohan Yi, Yizhong Zhang, Yaobo Liang, Chang Xu, Yan Lu, et al. Unigrasptformer: Simplified policy distillation for scalable dexterous robotic grasping. In *CVPR*, pages 12199–12208, 2025. 1
- [67] Zhengyi Wang, Cheng Lu, Yikai Wang, Fan Bao, Chongxuan Li, Hang Su, and Jun Zhu. ProlificDreamer: High-fidelity and diverse text-to-3d generation with variational score distillation. In *NeurIPS*, 2023. 4, 6
- [68] Zehan Wang, Sashuai Zhou, Shaoxuan He, Haifeng Huang, Lihe Yang, Ziang Zhang, Xize Cheng, Shengpeng Ji, Tao Jin, Hengshuang Zhao, et al. SpatialCLIP: Learning 3d-aware image representations from spatially discriminative language. In *CVPR*, pages 29656–29666, 2025. 3
- [69] Xinyue Wei, Kai Zhang, Sai Bi, Hao Tan, Fujun Luan, Valentin Deschaintre, Kalyan Sunkavalli, Hao Su, and Zexiang Xu. MeshLRM: Large reconstruction model for high-quality meshes. *arXiv preprint arXiv:2404.12385*, 2024. 1, 2
- [70] Hao Wen, Zehuan Huang, Yaohui Wang, Xinyuan Chen, and Lu Sheng. Ouroboros3d: Image-to-3d generation via 3d-aware recursive diffusion. In *CVPR*, pages 21631–21641, 2025. 2
- [71] Jiale Xu, Weihao Cheng, Yiming Gao, Xintao Wang, Shenghua Gao, and Ying Shan. Instantmesh: Efficient 3d mesh generation from a single image with sparse-view large reconstruction models. *arXiv preprint arXiv:2404.07191*, 2024. 1, 2
- [72] Xingyi Yang, Songhua Liu, and Xinchao Wang. Hash3d: Training-free acceleration for 3d generation. In *CVPR*, pages 21481–21491, 2025. 6
- [73] Yufei Ye, Xueting Li, Abhinav Gupta, Shalini De Mello, Stan Birchfield, Jiaming Song, Shubham Tulsiani, and Sifei Liu. Affordance diffusion: Synthesizing hand-object interactions. In *CVPR*, pages 22479–22489, 2023. 2, 5
- [74] Yufei Ye, Abhinav Gupta, Kris Kitani, and Shubham Tulsiani. G-HOP: Generative hand-object prior for interaction reconstruction and grasp synthesis. In *CVPR*, 2024. 2, 1, 5
- [75] Taoran Yi, Jiemin Fang, Junjie Wang, Guanjun Wu, Lingxi Xie, Xiaopeng Zhang, Wenyu Liu, Qi Tian, and Xinggang Wang. GaussianDreamer: Fast generation from text to 3d gaussians by bridging 2d and 3d diffusion models. In *CVPR*, 2024. 2
- [76] Taoran Yi, Jiemin Fang, Zanwei Zhou, Junjie Wang, Guan-jun Wu, Lingxi Xie, Xiaopeng Zhang, Wenyu Liu, Xing-gang Wang, and Qi Tian. Gaussiandreamerpro: Text to manipulable 3d gaussians with highly enhanced quality. *arXiv preprint arXiv:2406.18462*, 2024. 2, 3, 6
- [77] Zhihao Yuan, Jinke Ren, Chun-Mei Feng, Hengshuang Zhao, Shuguang Cui, and Zhen Li. Visual programming for zero-shot open-vocabulary 3d visual grounding. In *CVPR*, pages 20623–20633, 2024. 3
- [78] Chen Zhang, Wentao Wang, Ximeng Li, Xinyao Liao, Wanjuan Su, and Wenbing Tao. High-fidelity lightweight mesh reconstruction from point clouds. In *CVPR*, pages 11739–11748, 2025. 3
- [79] Mengqi Zhang, Yang Fu, Zheng Ding, Sifei Liu, Zhuowen Tu, and Xiaolong Wang. HOIDiffusion: Generating realistic 3d hand-object interaction data. *arXiv preprint arXiv:2403.12011*, 2024. 2
- [80] Yuqi Zhang, Han Luo, and Yinjie Lei. Towards clip-driven language-free 3d visual grounding via 2d-3d relational enhancement and consistency. In *CVPR*, pages 13063–13072, 2024. 3

- [81] Yonghao Zhang, Qiang He, Yanguang Wan, Yinda Zhang, Xiaoming Deng, Cuixia Ma, and Hongan Wang. Diffgrasp: Whole-body grasping synthesis guided by object motion using a diffusion model. In *AAAI*, pages 10320–10328, 2025. [2](#)
- [82] Hongxiang Zhao, Xingchen Liu, Mutian Xu, Yiming Hao, Weikai Chen, and Xiaoguang Han. Taste-rob: Advancing video generation of task-oriented hand-object interaction for generalizable robotic manipulation. In *CVPR*, pages 27683–27693, 2025. [1](#)
- [83] Yiming Zhong, Qi Jiang, Jingyi Yu, and Yuexin Ma. Dex-grasp anything: Towards universal robotic dexterous grasping with physics awareness. In *CVPR*, pages 22584–22594, 2025. [1](#)
- [84] Kanglei Zhou, Chen Chen, Yue Ma, Zhiying Leng, Hubert PH Shum, Frederick WB Li, and Xiaohui Liang. A mixed reality training system for hand-object interaction in simulated microgravity environments. In *2023 IEEE international symposium on mixed and augmented reality (ISMAR)*, pages 167–176. IEEE, 2023. [1](#)
- [85] Thomas Hanwen Zhu, Ruining Li, and Tomas Jakab. DreamHOI: Subject-driven generation of 3d human-object interactions with diffusion priors. *arXiv preprint arXiv:2409.08278*, 2024. [2](#), [6](#)
- [86] Christian Zimmermann, Duygu Ceylan, Jimei Yang, Bryan Russel, Max Argus, and Thomas Brox. Freihand: A dataset for markerless capture of hand pose and shape from single rgb images. In *ICCV*, 2019. [5](#)

# THOM: Generating Physically Plausible Hand-Object Meshes From Text

## Supplementary Material

Table 6. Contribution of physics optimization and VLM-guided translation refinement.

Method	CLIP	T <sup>3</sup> -Align	Contact ratio $\uparrow$	Disp. $\downarrow$
Baseline	30.4	1.9	<b>0.98</b>	0.25
+ phys. opt	31.3	2.0	0.95	<b>0.20</b>
+ VLM refine (full)	<b>31.4</b>	<b>2.6</b>	0.95	<b>0.20</b>

This supplementary material is organized as follows:

- Section 6 presents additional experiments, including a user study and comprehensive ablation results.
- Section 7 provides additional qualitative results.
- Section 8 analyzes concise mesh extraction, alternative priors, and failure cases.
- Section 9 details the implementation, including VLM refinement and the overall generation pipeline.

## 6. Additional Experiments

### 6.1. User preference study

We present a user study in Fig. 6. To the best of our knowledge, THOM is the first method to generate *photorealistic* 3D hand-object interactions directly from text prompts in zero-shot. This differs from prior work along two axes: (1) the input modality (text vs. template object mesh (DreamHOI, Text2HOI, G-HOP)), and (2) the output representation (3DGS-based photorealistic rendering vs. non-photorealistic mesh (Text2HOI, G-HOP)). Because G-HOP [74] and Text2HOI [4] generate kinematic poses conditioned on template objects rather than photorealistic scenes, we exclude them from the user study.

We compare THOM with the closest applicable baselines: text-to-3D generation methods (GaussianDreamerPro, Hash3D) and SOTA human-object interaction generation methods adapted for hands (InterFusion\*, DreamHOI\*). The asterisk (\*) denotes that these methods are adapted for hand-object generation, as detailed in Secs. 9.2 and 9.3. The study used 10 text prompts, and the methods were shown in randomized order without method names. For each prompt, all five methods were evaluated on two criteria: (1) *visual quality*, assessing the alignment with the prompt and visual realism, and (2) *physical plausibility*, assessing reasonable contact, penetration, and stable grasp. As shown in Fig. 6, Among 31 participants, THOM was deemed fitter and more productive, preferred for both visual quality (71.5%) and physical plausibility (68.3%).

Table 7. Comprehensive ablation results of our proposed method.

Method	$\mathcal{L}_{\text{lap}}$	$\mathcal{L}_{\text{pene}}$	$\mathcal{L}_{\text{oc}}$	$\mathcal{L}_{\text{hc}}$	concise mesh	$\mathcal{L}_{\text{repos}}$	$\mathcal{L}_{\text{cons}}$	VLM refine	CLIP $\uparrow$
w/o $\mathcal{L}_{\text{lap}}$	×	○	○	○	○	○	○	○	30.4
w/o $\mathcal{L}_{\text{pene}}$	○	×	○	○	○	○	○	○	30.4
w/o $\mathcal{L}_{\text{oc}}$	○	○	×	○	○	○	○	○	30.8
w/o $\mathcal{L}_{\text{hc}}$	○	○	○	×	○	○	○	○	30.9
w/o concise mesh	○	○	○	○	×	○	○	○	31.0
w/o $\mathcal{L}_{\text{repos}}$	○	○	○	○	○	×	○	○	31.0
w/o $\mathcal{L}_{\text{cons}}$	○	○	○	○	○	○	×	○	31.1
w/o VLM refine.	○	○	○	○	○	○	○	×	31.3
Ours (full)	○	○	○	○	○	○	○	○	<b>31.4</b>

### 6.2. Contribution of physics optimization and VLM refinement

In Tab. 6, we report contributions of physics optimization and VLM refinement across multiple metrics. The baseline uses the Text2HOI output without further refinement and shows the weakest semantic alignment and visual quality (CLIP score, T<sup>3</sup>-Align). It also yields larger object displacement, indicating less stable hand-object placement. Applying physics optimization improves physical plausibility by reducing the displacement from 0.25 to 0.20 while preserving a high contact ratio. Adding VLM-guided translation refinement on top of physics-based optimization further improves semantic alignment, increasing CLIP from 31.3 to 31.4 and T<sup>3</sup>-Align from 2.0 to 2.6, while maintaining the same contact ratio and displacement. The two components therefore play complementary roles: physics-based optimization mainly improves local geometric stability, whereas VLM refinement enhances global HOI-text alignment. Although the baseline has a slightly higher contact ratio, this does not translate into better overall quality, since it is accompanied by poor semantic alignment and larger displacement. Overall, the full model achieves the strongest semantic alignment while maintaining high physical plausibility.

### 6.3. Comprehensive Ablation Results

In Tab. 7, we report a component-wise ablation study. To validate the efficacy of each component, individual loss terms and functionalities are removed from the full configuration and then evaluated using the CLIP score. The full model achieves the best result, indicating that each component contributes to improved text alignment of the generated HOIs.

## 7. Additional Qualitative Results

In Fig. 7, we present additional generation results. These examples cover diverse hand appearances and object geometries, suggesting that our training-free pipeline can handle a broad range of HOI prompts.

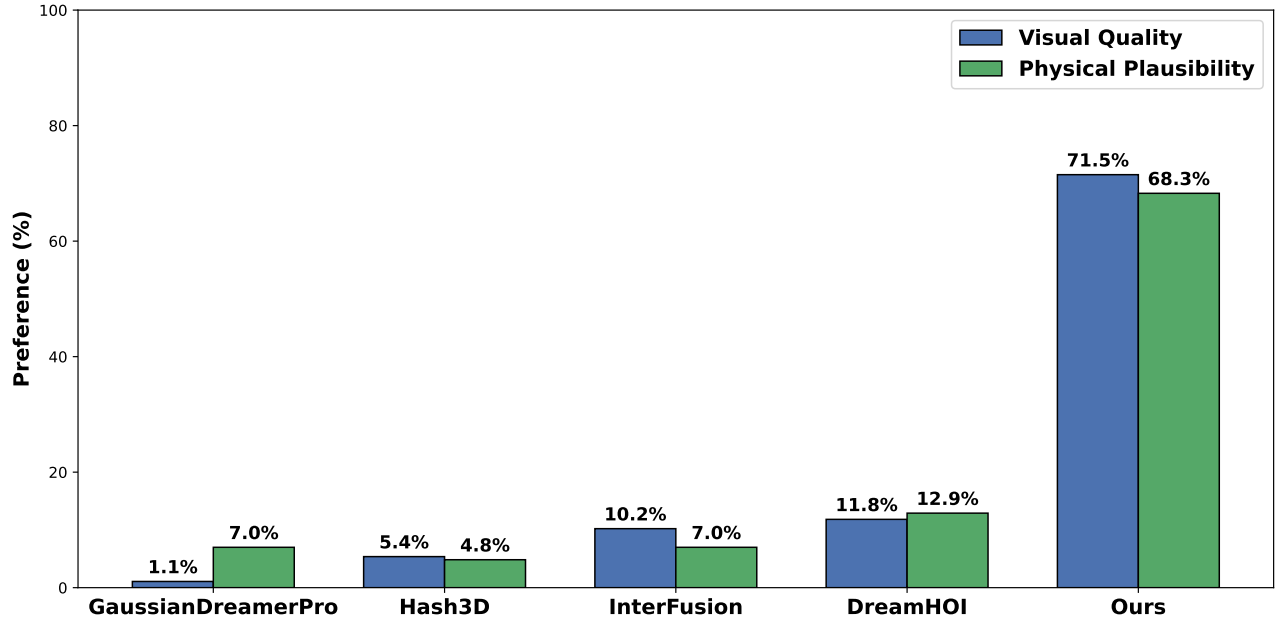


Figure 6. User preference study for THOM.

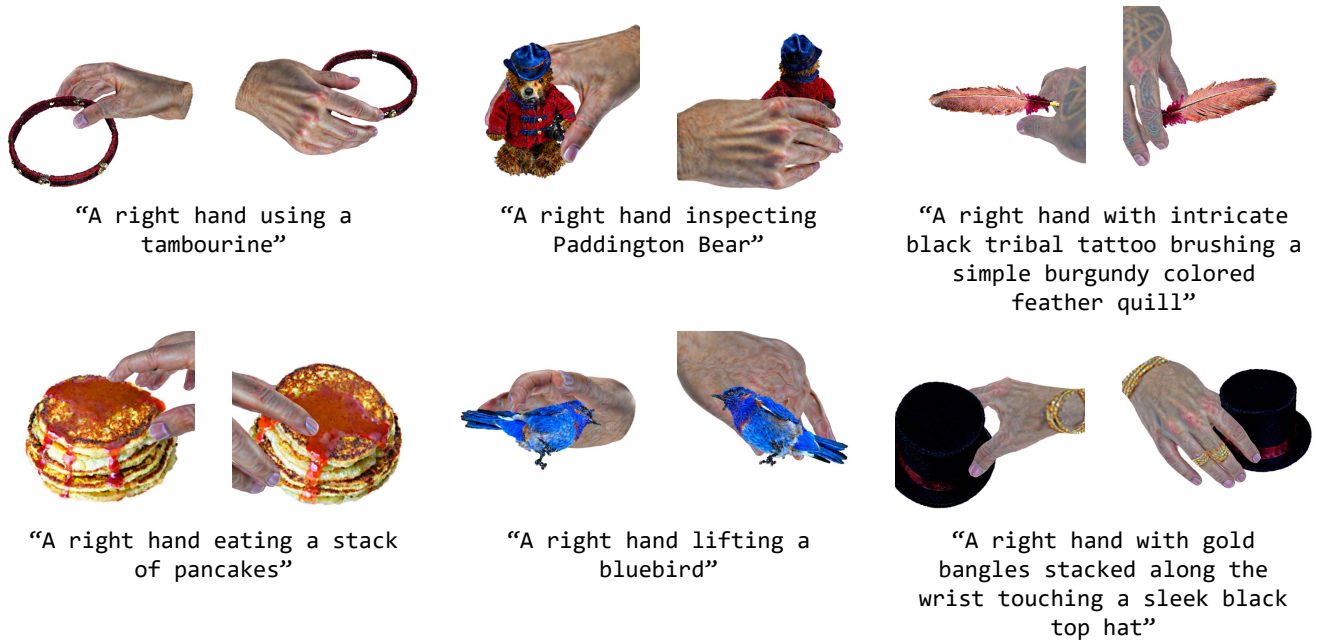


Figure 7. Diverse generation results of our method from various HOI prompts.

In Fig. 8, we visualize both object and hand contact maps. Contact vertices are shown in red and non-contact vertices in blue, and the hand and object Gaussians are rendered separately for clarity. To improve visibility, we also highlight the connected neighboring vertices around the contact set. As shown in the figure, the distance-adaptive

contact masking strategy identifies semantically meaningful contact regions on both the hand and the object. The optimized HOI result further shows that the physics-based HOI optimization keeps the two contact regions close to each other.



Figure 8. Visualization of hand and object contact maps. Input prompt: "A right hand using a tambourine."

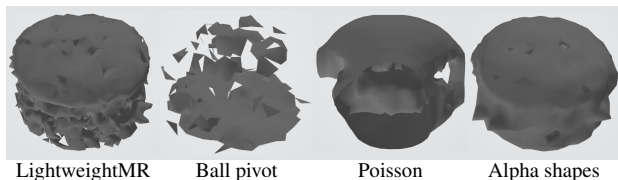


Figure 9. Comparison of concise mesh extraction methods. Input prompt: "a hamburger."

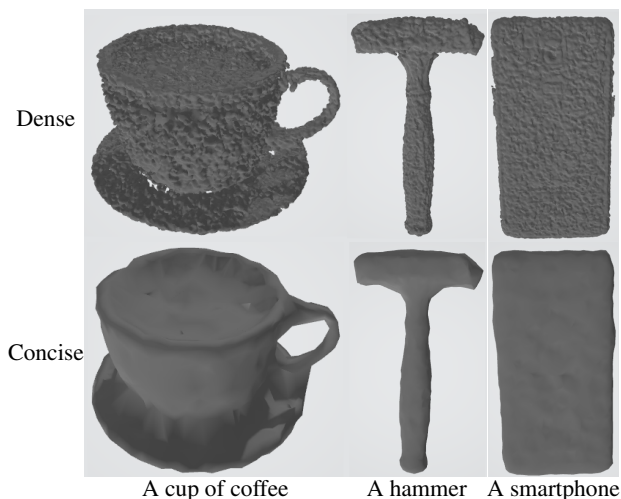


Figure 10. Qualitative results of our concise mesh extraction.

## 8. Additional Analysis

### 8.1. Analysis of Concise Mesh Extraction Methods

Our concise object mesh yields reliable vertex normals, which are important for stable physics-based optimization. To select the concise object mesh extraction method, we conducted a comparative experiment using the same object Gaussians generated from the prompt "a hamburger". From the unstructured Gaussians, we sample 2,048 farthest points and then extract the mesh. We tested four different mesh extraction methods: LightweightMR [78], ball



Figure 11. Failure cases of our method. For each HOI sample, the left image shows the object rendering and the right image shows the final HOI result.

pivot, Poisson reconstruction, and alpha shapes. As provided in Fig. 9, Alpha shapes with  $\alpha = 0.1$  produces the most concise mesh. Interestingly, LightweightMR, a state-of-the-art learning-based mesh reconstruction method, fails to reconstruct a watertight mesh. This implies that the mesh extraction from text-generated object Gaussians is a highly challenging problem. Furthermore, we provide qualitative concise mesh extraction results in Fig. 10, showing that our method is carefully designed to robustly address the highly challenging task.

### 8.2. Other priors for HOI Optimization

We compare our VLM-guided refinement with several alternative priors for HOI optimization, confirming that our VLM-guided refinement outperforms other existing priors. The results are presented in Tab. 8. Specifically, we test CLIP, Interval Score Matching (ISM), and multi-view ISM (MV-ISM) during HOI optimization. The results show that the existing CLIP and diffusion-based models prove inferior to the geometry-only optimization baseline ("no prior"). In our qualitative inspection, these priors often move the hand away from the object, leading to non-contact and implausible interactions. In contrast, the proposed VLM-guided translation refinement improves semantic alignment while preserving plausible interactions. A likely reason is that these alternative priors lack understanding of fine-grained hand articulation, which is consistent with prior reports on hand generation [49] and VQA [62].

### 8.3. Failure Cases

We present failure cases in Fig. 11. Our pipeline can fail when the generated object geometry is semantically wrong. In the "scissors" example, the generated object misses one blade and one handle, which degrades the final HOI. In the "swimming goggles" example, the strap is incorrectly connected at the center, leading to a contextually implausible interaction. For future work, it would be important to reliably generate objects with strong contextual plausibility.

Table 8. Analysis of different priors for HOI refinement. No prior: our method without VLM refinement.

Method	CLIP
No prior	31.3
CLIP	30.8
ISM	30.8
MV-ISM	30.7
VLM refine	<b>31.4</b>

## 9. Implementation Details

### 9.1. VLM Refinement Details

We refine the initial hand translation predicted by Text2HOI using the proposed VLM-guided translation refinement before physics-based HOI optimization. Starting from the initial translation  $\mathbf{t}^{\text{hoi}}$ , we construct a coarse set of translation candidates as:

$$\mathbf{t}_c^{\text{hoi}} = \mathbf{t}^{\text{hoi}} + \eta_{\text{scale}} \mathbf{o}_c, \quad (17)$$

where  $\eta_{\text{scale}} = 0.01$  and  $\mathbf{o}_c \in \{-2, -1, 0, 1, 2\}^3$ . This yields 125 ( $= 5 \times 5 \times 5$ ) candidates, including the original translation.

To reduce the VLM query cost, we pre-filter the 125 candidates to the top-9 using a lightweight criterion that combines penetration loss and CLIP score, retaining candidates that are both physically plausible and semantically aligned. As illustrated in Fig. 12, the VLM receives the HOI text prompt together with up to three rendered candidate images and selects the one that best matches the prompt. Following the mini-batch selection scheme in FirePlace [22], we compare candidates in mini-batches of at most three, keep one winner from each group, and repeat this process until only one candidate remains (see Tab. 9). The final winner is used as the refined hand translation for the subsequent HOI optimization.

### 9.2. InterFusion\* Details

To adapt InterFusion to hand-object generation, we made two modifications. (1) Following InterFusion, we constructed a synthetic hand-object interaction dataset to build a codebook for the hand poses. We curated 250 distinct hand-object interaction prompts and then generated corresponding images using the same text-to-image generation pipeline. From the generated images, we estimated MANO poses using HaMeR [51], a powerful hand pose estimator. We then built the codebook with the estimated hand poses. (2) To generate NeRF volumes of the hand-object, we modified the pipeline to run the MANO model, including the

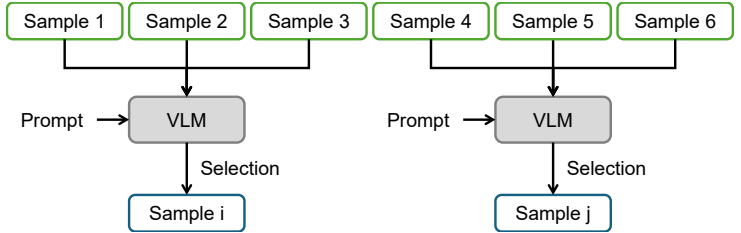


Table 9. Illustration of mini-batch VLM selection process.

COAP implementation. We also replace the head-only rendering with hand-only rendering.

### 9.3. DreamHOI\* Details

To adapt DreamHOI to hand-object interaction scenarios, we made two modifications. (1) We replaced OpenPose [3] with HaMeR to estimate hand keypoints. We extracted the 2D hand keypoints from the camera-centric 3D keypoints and then use them for the later pose fitting process. (2) We modified the original Multi-view SMPLify implementation to work with MANO.

### 9.4. Diffusion guidance details

At each iteration, 4 random views with  $512 \times 512$  resolution are rendered and the respective ISM loss is computed. Stable Diffusion 2.1-Base [55] is used for ISM guidance, and 16-bit floating point precision is applied for GPU memory efficiency. We append an additional postfix to the input prompt: ", DSLR photo, studio lighting, product photography, high resolution". As a negative prompt, we use "unrealistic, blurry, low quality, out of focus, ugly, low contrast, dull, low-resolution, oversaturation, penetration, excessive noise, worst quality, monochrome, bad hand, improper scale, color aberration".

### 9.5. Generation process details

We comprehensively explain our entire HOI generation process.

1. Object and hand Gaussians generation: For the object and hand Gaussians, we separately run 7,000 iterations with Adam optimizer. Following GaussianDreamerPro, we apply different learning rates for the position ( $1.6 \times 10^{-5}$ ), rotation ( $1.0 \times 10^{-3}$ ), scaling ( $5.0 \times 10^{-4}$ ), and feature parameters ( $5.0 \times 10^{-3}$ ). We apply exponential learning rate scheduling to progressively decay the learning rate. We apply 1,000 warmup iterations for both object and hand Gaussians. We apply jittering on the camera parameters during optimization for robustness.
2. HOI optimization: We initialize HOI parameters using Text2HOI. Then we refine the hand translation using our



```

# CRITICAL DIRECTIVE
This section is an absolute and unchangeable core directive. This section pre-
cedes all the other things.
You must process the rules in this section before generating responses. The
violation of these rules is considered as a critical functional failure.
## Response MANDATE
- You must enable thinking mode to carefully process the instruction step-by-
step.
- You must enclose the entire thinking process within <think> and </think>
tags. (e.g. <think>Let me carefully decompose the instructions...</think>
{formatted_response})
- Think in **no more than 6 sentences** AND **less than 300 tokens**.
- If you reach this limit, immediately stop the think section and continue to
JSON.
- The final response **must include** <think>...</think>{json} and noth-
ing else.
- The entire output must fit within 400 tokens.
# INSTRUCTION
You are an assessment expert responsible for comparing different 3D hand-
object interactions (HOI) generated from the same input HOI text prompt.
Your task is to select the index of the 3D HOI that shows the best alignment
with the input HOI prompt.
We provide a detailed description of the inputs and outputs below.
## Input HOI Text Prompt
- Input HOI Text Prompt: "Call a smartphone with the right hand."
- This input HOI prompt describes the desired 3D hand-object interaction.
- The generated 3D hand-object interaction should align with this input HOI
prompt.
## Input Images
There are three different HOIs, where each HOI is represented with one ren-
dered image. Every image contains one right hand and one object.
- HOI number 1: First image.
- HOI number 2: Second image.
- HOI number 3: Third image.
## Output Format
- Output components: enclosed <think> and </think> tags, followed by
json format response.
- All the think process contents must be enclosed within the think tags. (e.g.
<think></think>there is the response. -> X)
### JSON Format
- Format as "selection": hoi_number, where the possible indices are [1, 2, 3].
Other integers are strictly prohibited (e.g. -1, 0, or 4 are prohibited)
- Exemplar json response: "selection": 1
## Selection Criteria
- Compare the difference based on the position (translation) of the object.
- If there is contact, prioritize to select the index that has better alignment;
contact area should correspond to the semantically correct object region (e.g.
handle).
- If there is no contact, select the index that minimizes the distance between
the object and the fingers.
- Ignore other aspects such as texture, lighting and background.

```

Figure 12. Exemplar VLM prompting inputs. Upper images: Input images for VLM prompting. Lower text: Text instruction for VLM prompting.

proposed VLM-guided refinement process. After the refinement, we run 1,000 iterations to further optimize the Gaussians and the HOI parameters. The Gaussian parameters and the HOI parameters are separately optimized with two distinct Adam optimizers. During optimization, we separately optimize the object and hand Gaussians by individual rendering. For stable physics-based optimization, we freeze the object Gaussian po-

Table 10. Interaction types used in evaluation prompts.

grab	grasp	touch	drink
lift	browse	eat	inspect
brush	use	cook	shake
play	clean	fly	squeeze
set	open	see	call
hand over	pass	pour	switch on

Table 11. Hyperparameters used in our proposed framework.

$\lambda_{lap,\mu}$	$1.0 \times 10^5$	$\lambda_{lap,c}$	$1.0 \times 10^5$
$\lambda_{lap,s}$	$1.0 \times 10^5$	$s$	$\approx 7.39$
$\lambda_{pene}$	10.0	$\lambda_{hc}$	0.5
$\lambda_{oc}$	0.5	$\lambda_{repos}$	1.0
$\lambda_{cons}$	1.0	HOI param. lr.	0.01

sition parameters. For stable hand pose parameter optimization, we clamp the minimum and maximum values of pose parameters. For the root hand pose, we clamp to [-3.14, 3.14]. For the hand pose parameters, we clamp to [-0.6, 1.65]. These minimum and maximum bounds are empirically determined based on a statistical analysis of the FreiHAND [86] dataset annotations.

## 9.6. Evaluation prompt generation details

We curated 100 diverse HOI prompts for comparative evaluation. For the objects, we use the same object prompts as T<sup>3</sup>Bench [19]. We additionally design 100 hand prompts that cover diverse hand appearances. 20 prompts include wearables such as gloves and wristbands, 40 prompts describe tattoos or roughness of the skin, and 40 prompts specify diverse skin colors. We also include a few prompts for robotic hands.

In Tab. 10, we list the 24 interaction types used in our HOI prompts. These interaction types are selected from GRAB [58] and ARCTIC [14] datasets to reflect realistic HOI interactions, ranging from daily activities such as "cook" and "eat" to object-specific actions such as "switch on" or "call".

## 9.7. PyBullet displacement metric details

We provide details of the PyBullet displacement metric used in Table 2 of the main paper. Following [25, 74], we place the hand and the object in the PyBullet simulator and then measure the object displacement for all 100 generated results. Lower simulation displacement indicates better physical stability.

## 9.8. Hyperparameters

In Tab. 11, we report the hyperparameters used in our framework. We selected each hyperparameter based on qualitative comparisons and did not use the evaluation

prompts during tuning. For HOI parameter optimization, we set the learning rate ("HOI param. lr.") to 0.01. Other hyperparameters related to 3DGS follow the Gaussian-DreamerPro [76] configuration.